IEEE TRANSACTIONS ON
ENERGY CONVERSION
IEEE POWER & ENERGY SOCIETY

Stable Short-Term Frequency Support Using Adaptive Gains for a DFIG-Based Wind Power Plant

Jinsik Lee, *Student Member, IEEE*, Gilsoo Jang, *Senior Member, IEEE*, Eduard Muljadi, Frede Blaabjerg, *Fellows, IEEE*, Zhe Chen, and Yong Cheol Kang, *Senior Members, IEEE*

***Abstract*—For the fixed-gain inertial control of wind power plants (WPPs), a large gain setting provides a large contribution to supporting system frequency control, but it may cause over-deceleration for a wind turbine generator (WTG) that has a small amount of kinetic energy (KE). Further, if the wind speed decreases during inertial control, even a small gain may cause over-deceleration. This paper proposes a stable inertial control scheme using adaptive gains for a doubly-fed induction generator (DFIG)-based WPP. The scheme aims to improve the frequency nadir (FN) while ensuring stable operation of all DFIGs, particularly when the wind speed decreases during inertial control. In this scheme, adaptive gains are set to be proportional to the KE stored in DFIGs, which is spatially and temporally dependent. To improve the FN, upon detecting an event, large gains are set to be proportional to the KE of DFIGs; to ensure stable operation, the gains decrease with the declining KE. The simulation results demonstrate that the scheme improves the FN while ensuring stable operation of all DFIGs in various wind and system conditions. Further, it prevents over-deceleration even when the wind speed decreases during inertial control.**

***Index Terms*—Inertial control, releasable kinetic energy (KE), fixed-gain scheme (FGS), adaptive-gain scheme (AGS), frequency nadir (FN), over-deceleration.**

I. Introduction

System frequency indicates the balance between the power generation and consumption in an electric power grid and should be maintained within an allowable range at all times to ensure stable operation. If a frequency event occurs, synchronous generators (SGs) inherently release part of the kinetic energy (KE) stored in their rotating masses, then the SGs that have operating reserve participate in primary and secondary controls by increasing their active power [1]. If system frequency decreases below the predefined value, an under-frequency relay sheds part of the load to prevent a further decrease; thus, the frequency nadir (FN) is an important metric for determining grid reliability [2].

Variable-speed wind turbine generators (WTGs) are widely used because they can perform maximum power point tracking (MPPT) operation and provide advanced control functions by using converters. However, the MPPT function causes them not to respond to the system frequency variation; thus, a significant frequency reduction is inevitable if an event occurs in an electric power grid. To minimize this problem, the grid codes in some countries require inertial response from a large-scale wind power plant (WPP) [3].

Many researchers have reported on the inertial control schemes of variable-speed WTGs that temporarily releases the KE stored in their rotating masses to arrest the FN [4]−[12]. To do this, these schemes employ additional loops based on the measured frequency: rate of change of frequency (ROCOF) loop [4]−[6], droop loop [7], and ROCOF and droop loops [8]−[12]. They can arrest the FN by releasing part of the stored KE; however, in these schemes, control gains are set to be fixed, and thus difficulty arises in finding a fixed gain of a WTG suitable for various wind conditions. Comprehensive analysis on the effects of different gains on the performance of inertial control has been addressed [6], [10]−[12]. A large gain can improve the FN while preventing over-deceleration of a WTG, which causes an overvoltage and/or stall, only if a WTG has sufficient KE. Conversely, a small gain can prevent over-deceleration, but it provides a limited contribution to improving the FN. In addition, if the fixed-gain scheme (FGS) is applied to a WPP consisting of multiple WTGs, difficulties will arise in setting the fixed and same gain suitable for all WTGs, which have different amounts of stored KE because of the wake effects. This means that a large gain is suitable for a WTG that has a large level of KE, but it is unsuitable for a WTG that has a small level of KE, and vice versa. Further, if the wind speed decreases in the middle of inertial control, even a small gain may be unable to prevent over-deceleration.

This paper proposes a stable inertial control scheme using adaptive gains for a doubly-fed induction generator (DFIG) -based WPP. The proposed scheme aims to improve the FN while ensuring stable operation of all DFIGs, especially if the wind speed decreases during inertial control. In this scheme, adaptive gains are set to be proportional to the KE stored in a DFIG, which is spatially and temporally dependent. To improve the FN, at the instant of an event, large gains are

This work was supported by the National Research Foundation of Korea grant funded by the Korea government (MSIP) (No. 2010-0028509). NREL's contribution to this work was supported by the U.S. Department of Energy under Contract No. DE-AC36-08-GO28308 with the NREL.

Jinsik Lee is with the Department of Electrical Engineering and Wind energy Grid-Adaptive Technology (WeGAT) Research Center, Chonbuk National University, Korea (e-mail: jinsiklee@jbnu.ac.kr).

Gilsoo Jang is with the School of Electrical Engineering, Korea University, Korea (e-mail: gjang@korea.ac.kr).

Eduard Muljadi is with the National Renewable Energy Laboratory, CO, USA (e-mail: eduard.muljadi@nrel.gov).

Frede Blaabjerg and Zhe Chen are with the Department of Energy Technology, Aalborg University, Denmark (e-mails: fbl@et.aau.dk and zch@et.aau.dk).

Yong Cheol Kang is with the Department of Electrical Engineering, WeGAT Research Center, and Smart Grid Research Center, Chonbuk National University, Korea (corresponding author to provide phone: +82-63-270-2391; fax: +82-63-270-2394; e-mail: yckang@jbnu.ac.kr).

initially set to be proportional to the KE, which is spatially dependent; then, to ensure stable operation, they temporally decrease with the declining KE. The performance of the proposed adaptive-gain scheme (AGS) is investigated under various wind and system conditions using an EMTP-RV simulator.

II. Proposed Stable Inertial Control Using Adaptive Gains for a DFIG-Based WPP

This section briefly describes the DFIG model used in this paper and the conventional fixed-gain inertial control scheme; then the overall features of the proposed AGS are described.

A. DFIG Model

Fig. 1(a) shows a typical configuration of the DFIG model used in this paper, which consists of a mechanical power model, two-mass shaft model, induction generator, and DFIG controller; in addition, Fig. 1(b) shows a pitch control scheme used in this paper.

The mechanical input power extracted from the wind, P_m, is defined by

$$P_m = \frac{1}{2}\rho A v_{wind}^3 c_P(\lambda,\beta) \tag{1}$$

where ρ, A, v_{wind}, c_P, λ, and β are the air density, rotor-swept area of a WTG in m^2, wind speed, power coefficient, tip-speed ratio, and pitch-angle, respectively.

As in [13], this paper uses $c_P(\lambda, \beta)$, as

$$c_P(\lambda,\beta) = 0.645\{0.00912\lambda + \frac{-5-0.4(2.5+\beta)+116\lambda_i}{e^{21\lambda_i}}\} \tag{2}$$

where

$$\lambda_i = \frac{1}{\lambda+0.08(2.5+\beta)} - \frac{0.035}{1+(2.5+\beta)^3} \tag{3}$$

From (2), the maximum c_P and optimum λ are set to 0.5 and 9.95, respectively.

A two-mass model for the mechanical dynamics of a wind turbine is represented by

$$\left.\begin{aligned} 2H_t\frac{d\omega_t}{dt} &= T_t - K_s\theta_s - D_s(\omega_t-\omega_g) - D_t\omega_t \\ 2H_g\frac{d\omega_g}{dt} &= K_s\theta_s + D_s(\omega_t-\omega_g) - D_g\omega_g - T_g \\ \frac{d\theta_s}{dt} &= \omega_0(\omega_t-\omega_g) \end{aligned}\right\} \tag{4}$$

where H_t, H_g, D_t, D_g, ω_t, ω_g, T_t, and T_g are inertia time constants, damping constants, angular speeds, and torques of a wind turbine and a generator mass, respectively; K_s, D_s, θ_s, and ω_0 are the shaft stiffness, damping constant, torsional twist, and base value of angular speed, respectively.

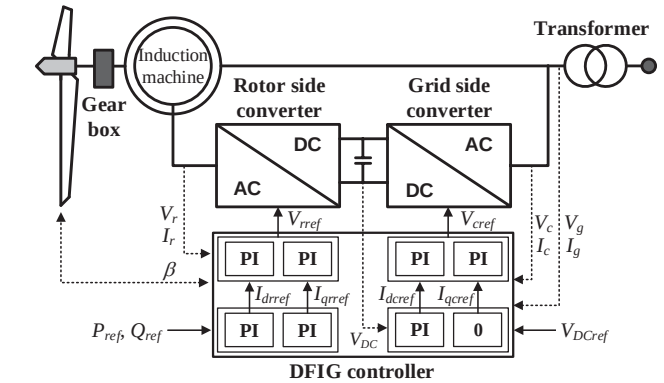

V_r, I_r: voltage and current at rotor circuit
V_g, I_g: voltage and current at terminal
I_{drref}, I_{qrref}: reference RSC current
V_{rref}: reference RSC voltage
V_c, I_c: voltage and current at GSC
V_{DC}: DC-link voltage
I_{dcref}, I_{qcref}: reference GSC current
V_{cref}: reference GSC voltage

(a) Typical configuration of a DFIG

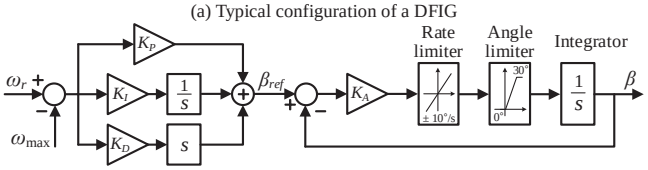

(b) Pitch control scheme (K_P = 180, K_I = 25, K_D = 25, K_A = 2)

Fig. 1. Typical configuration and pitch control scheme of a DFIG

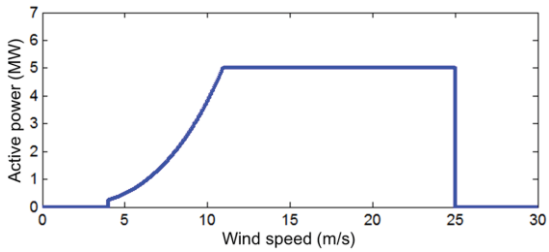

Fig. 2. Power curve of the DFIG used in this paper

Fig. 2 and Table I show the power curve and parameters of a DFIG used in this paper [14]. The cut-in, rated, and cut-out wind speeds are 4 m/s, 11 m/s, and 25 m/s, respectively. Fig. 3 illustrates the mechanical input and electrical output characteristics of a DFIG and the power and torque limits. The black solid lines are the mechanical power at different wind speeds. The dashed red line represents the MPPT curve, which is proportional to the cube of the rotor speed: $k_g\omega_r^3$, where k_g is set to 0.512 to produce the rated power at the maximum rotor speed. To obtain realistic simulation results, the power and torque limits are considered in this paper; the former is set to 1.20 p.u. [15], whereas the latter is set to 1.17 p.u. In addition, in this paper the minimum and maximum operating speed limits, $\omega_{\min}$ and $\omega_{\max}$, are set to 0.70 p.u. and 1.25 p.u., respectively.

A DFIG controller determines the reference voltages for the rotor-side converter (RSC) that regulates the active and reactive powers injected into the grid and for the grid-side converter (GSC) that maintains the DC-link voltage. To generate the references, the voltages and currents at the rotor circuit and the stator terminal of a DFIG and the rotor speed are measured. In addition, a pitch-angle controller is used to prevent the rotor speed from exceeding $\omega_{\max}$. An error signal between $\omega_{\max}$ and

TABLE I
DFIG PARAMETERS

	Units	Values
Nominal Apparent Power	MVA	6
Nominal Active Power	MW	5
Nominal Stator Voltage	kV	2.3
Stator Resistance	p.u.	0.023
Stator Leakage Reactance	p.u.	0.18
Magnetizing Reactance	p.u.	2.9
Rotor Resistance	p.u.	0.016
Rotor Leakage Reactance	p.u.	0.16
Operating Speed Range	p.u.	0.70−1.25

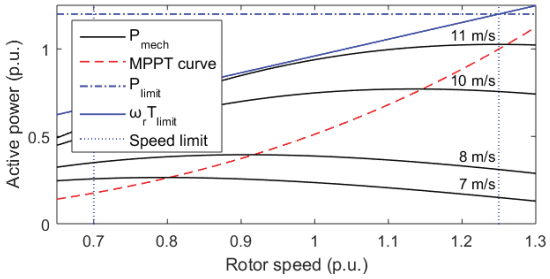

Fig. 3. Mechanical input and electrical output power characteristics of a DFIG

ω_r is passed through a proportional-integral-derivative controller. In addition, in this paper, the rate limiter and angle limiter are included; and the maximum pitch angle limit is set to 30° and the pitch rate is set to ±10°/s, as in [16].

B. Conventional Fixed-Gain Inertial Control Scheme

This subsection briefly describes a conventional fixed-gain inertial control scheme [8]−[12], which uses two additional loops: ROCOF and droop loops, as shown in Fig. 4. The top and bottom loops in Fig. 4 indicate the ROCOF and droop loops, respectively; K and $1/R$ are the control gains of the ROCOF and droop loops. The outputs of the ROCOF and droop loops, ΔP_{in} and ΔP, are added to the reference for MPPT control, P_{MPPT}, to generate the power reference of a DFIG, P_{ref}. Both loops mutually compensate the drawback of each loop, because ΔP_{in} is dominant during the initial stage of a disturbance, whereas ΔP is dominant around the FN.

C. Wake Effect Model

In this paper, the Park wake model, which is based on the Jensen wake model [17], is used to obtain the arriving wind speed at a WTG considering the wake effect. It assumes that the wake wind speed is linearly expanded, as shown in Fig. 5. The wake wind speeds at the WTGs are obtained by considering the cumulative impact of multiple shadowing and the effect of the wind direction [18]. The wind speed of WTG$_i$, V_i, can be obtained by using

$$V_i = V_0\left[1-\sqrt{\sum_{\substack{j=1\\ j\neq i}}^{n}\left\{2a_j\left(\frac{D_j}{D_j+2kx_{ji}}\right)^2\beta_{ji}\right\}^2}\right] \quad (5)$$

where V_0 is the free wind speed, β_{ji} is the ratio between the overlapping area and swept area of WTG$_i$, a_j is the axial induction factor of WTG$_j$, and n is the number of total WTGs.

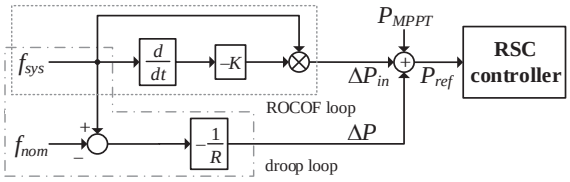

f_{nom}: nominal frequency f_{sys}: system frequency

Fig. 4. Conventional inertial control scheme of a DFIG [8]−[12]

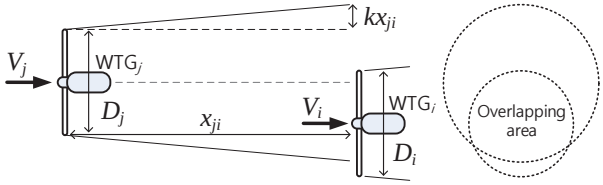

D_j: diameter of swept area of WTG$_j$ k: wake-decaying constant
x_{ji}: radial distance between WTG$_j$ and WTG$_i$

Fig. 5. Shadow cone

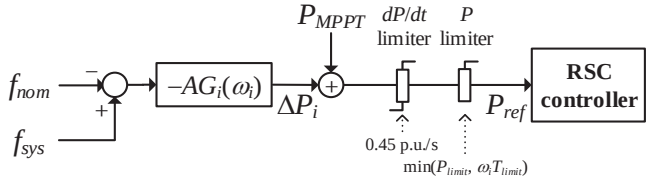

$AG_i(\omega_i)$: adaptive gain ΔP_i: reference from the frequency deviation loop
P_{ref}: power reference of a DFIG P_{MPPT}: reference for MPPT control

Fig. 6. Proposed adaptive-gain inertial control scheme of a DFIG

D. Proposed Adaptive-Gain Inertial Control Scheme for a DFIG-Based WPP

As mentioned in the introduction, if the FGS is applied to a WPP, difficulties arise in setting the fixed and same control gain suitable for all WTGs. The reason for this is as follows. WTGs within a WPP have different levels of KE because of the wake effects. A large gain for improving the FN might cause over-deceleration for a WTG that has a small amount of KE. Further, it may cause over-deceleration even for a WTG that has a large amount of KE if the wind speed decreases in the middle of inertial control.

The proposed AGS aims to (1) increase the FN and (2) ensure stable operation of all DFIGs during inertial control. In this scheme, only the frequency deviation loop is used as an additional control loop, because the ROCOF loop is vulnerable to noise components contained in the measured frequency. In addition, the slow response of the frequency deviation loop is overcome by setting large initial gains at the instant of an event, which depends on the KE stored in a DFIG. Fig. 6 shows the proposed adaptive-gain inertial control scheme. In the AGS, to achieve these objectives, the control gain of the frequency deviation loop of DFIG$_i$, $AG_i(\omega_i)$, is set to be proportional to the releasable KE of DFIG$_i$, ΔE_i, which is given as

$$AG_i(\omega_i) \propto \Delta E_i = H(\omega_i^2 - \omega_{\min}^2) \quad (6)$$

where H is an inertia time constant in seconds, and ω_i and $\omega_{\min}$ are the instantaneous rotor speed and the minimum rotor speed limit of DFIG$_i$, respectively.

Rewriting (6) gives

$$AG_i(\omega_i) = C(\omega_i^2 - \omega_{\min}^2), \quad for\ \omega_i < \omega_{\max}$$
$$AG_i(\omega_i) = C(\omega_{\max}^2 - \omega_{\min}^2), \quad for\ \omega_i \geq \omega_{\max} \tag{7}$$

where C is a constant.

In (7), ω_i and $AG_i(\omega_i)$ are spatially and temporally dependent variables. First, the meaning of the spatial dependency of the $AG_i(\omega_i)$ is described as follows. As mentioned in the previous subsection, each DFIG has a spatially different level of KE because of the wake effects. To improve the FN, during the early stage of an event, a larger gain is initially set for a DFIG that has a larger amount of KE, whereas a smaller gain is initially set for a DFIG that has a smaller amount of KE; in addition, at $\omega_i = \omega_{\min}$, the control gain is set to zero. This helps the AGS release more KE than the FGS during the initial stage of an event. Second, the meaning of the temporal dependency of the $AG_i(\omega_i)$ is as follows. ω_i keeps decreasing while performing inertial control because of the large initial gain setting, and it eventually causes over-deceleration. To avoid over-deceleration, in the AGS, $AG_i(\omega_i)$ is set to temporally decrease as ω_i declines. This ensures stable operation by preventing over-deceleration. Therefore, the proposed $AG_i(\omega_i)$ can improve the FN when initially set to be proportional to the spatially different KE, and it can prevent over-deceleration of all DFIGs by reducing the gains depending on the temporally decreasing KE.

C in (7) can be determined in many ways depending on the design purposes and system configuration. A C that is too large might cause a large power reduction rate after the FN and thereby may cause a second frequency dip even though over-deceleration can be prevented. Thus, C is set to 200 in this paper to increase the FN while avoiding a second frequency dip after the FN.

In addition, to obtain the realistic results, the limiter of the output power is used; the upper limit is set to the minimum value of the power and torque limitations, min(P_{limit}, $\omega_i T_{limit}$). In addition, to consider the mechanical stress, the rate limiter is used and set to 0.45 p.u./s [19].

III. Model System

A model system used for the simulation is shown in Fig. 7. To investigate the performance of the proposed inertial control scheme, a DFIG-based WPP and a grid consisting of six SGs and motor and static loads are modeled using an EMTP-RV simulator. Total generation capacity of the model system is 1,020 MVA, and the consumption is 529 MW.

A. SGs

To benchmark the Korean power system, which has a low ramping capability, in this paper all conventional SGs are modeled as steam turbine generators. There are two 100-MVA SGs, two 150-MVA SGs, and two 200-MVA SGs in the model system, and the inertia time constants are set to 4 s, 4.3 s, and 5 s, respectively, depending on the rated capacity [20]. Fig. 8 and Table II show the IEEEG1 steam governor model in [21] and its coefficients, respectively; and the droops for the SGs are set to 5%, which is the typical droop setting of the SGs used in the Korean power system.

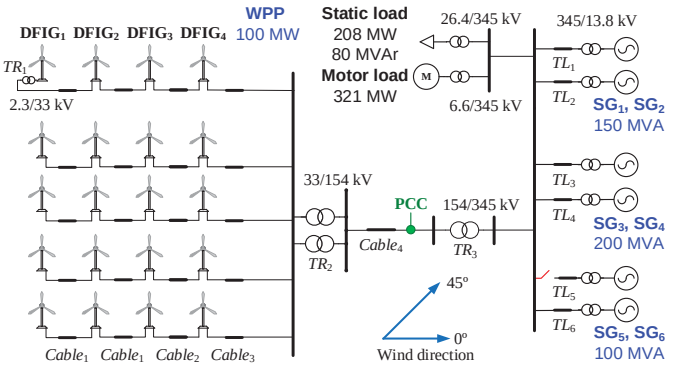

Fig. 7. Model system

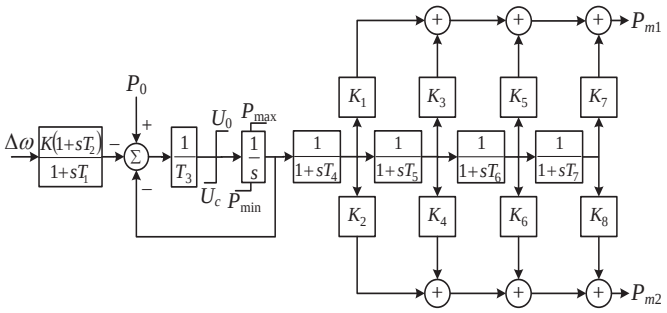

Fig. 8. IEEEG1 steam governor model

Secondary frequency control, known as automatic generation control, is not considered because it is beyond the scope of this paper; thus, the system frequency is not fully recovered to the nominal value after the frequency rebound.

B. DFIG-Based WPP

The WPP consists of 20 5-MW DFIGs. The distance between two DFIGs is 1,139 m, which is 9 D, where D is a diameter of the swept area of a wind turbine. Five feeders are connected to a collector bus, and each feeder has four DFIGs. The inner grid is connected through two 72-MVA substation transformers and a 22-km submarine intertie cable to the grid. The voltage level of the inner and outer grids is 33 kV and 154 kV, respectively.

In this paper, the DFIG estimates the system frequency to perform inertial control without the additional information from a higher level controller. To do this, the DFIG samples the terminal voltage at the sampling frequency of 3,840 Hz; the measured voltages are passed through a second-order, anti-aliasing, low-pass filter with a cutoff frequency of 1,920 Hz. In addition, a phase-locked loop is used to calculate the system frequency [22], and the rotor speed of the DFIG is measured to obtain the adaptive gain from (7). Inertia time constant for a 5-MW DFIG is set to 5 s in this paper. Table III shows the parameters of cables and transformers for inner and outer grids of the WPP.

C. System Loads

Typically, a motor load highly dependent on the system frequency has 60% to 70% in total loads of a typical electric

TABLE II

COEFFICIENTS OF THE IEEEG1 STEAM GOVERNOR MODEL

K	K_1	K_2	K_3	K_4	K_5	K_6	K_7	K_8	P_{MAX}
20	0.3	0	0.4	0	0.3	0	0	0	1
T_1	T_2	T_3	T_4	T_5	T_6	T_7	U_o	U_c	P_{MIN}
0.1	0	0.25	0.3	10	0.4	0	0.3	-0.5	0.33

TABLE III

PARAMETERS OF CABLES AND TRANSFORMERS

	Unit	$Cable_1$	$Cable_2$	$Cable_3$	$Cable_4$
Rated Voltage	kV	33	33	33	154
Cross-Section Area	mm^2	70	185	400	500
Resistance	Ω/km	0.344	0.130	0.064	0.056
Reactance	Ω/km	0.172	0.148	0.132	0.151
Capacitance	μF/km	0.117	0.160	0.209	0.141
	Unit	TR_1 (Y/△)	TR_2 (△/Y)	TR_3 (Y/Y)	
Rated Capacity	MVA	6.25	72	150	
Rated Frequency	Hz	60	60	60	
Turns Ratio	kV	2.3/33	33/154	154/345	
% Impedance	%	5.4	7	9	

power grid [23]. Thus, the motor load can also support the frequency control of a grid by reducing the consumption after a disturbance. To consider the operating characteristic of the motor load, in this paper 61% of the total load is implemented to the motor load, and the rest of the total load is static.

IV. CASE STUDIES

The performance of the proposed AGS was investigated by comparing it to the "FGS" with different fixed gains and "no inertial control" under various wind and system conditions in a model system. At 40 s, SG_5 supplying 70 MW is tripped as an event and the system frequency drops.

In the FGS, K is set to 10, as in [4], whereas $1/R$ is set to 45 and 18. The larger gain was selected so that it maximizes the inertial control performance while ensuring stable operation of all DFIGs in medium wind conditions; whereas the smaller gain was chosen so that it maximizes the FN while ensuring stable operation of all DFIGs in low wind conditions. Note that these gains provide only an example of the large or small FGS in the model system; they can be changed if the system is changed. At the instant of an event, the initial adaptive gains are set depending on spatially different levels of KE; afterward, adaptive gains decrease with the temporally declining KE by using (7).

In Case 1, Case 2, and Case 3 the wind speed is assumed to be constant during inertial control; whereas in Case 4 and Case 5 the wind speed is assumed to be reduced at the instant of an event, from 10 m/s to 7 m/s for 10 s and 1 s, respectively. In Case 6 the wind power penetration level increases from 19% to 30% for the wind speed of 10 m/s. Table IV and Table V represent the wind speeds of all DFIGs obtained by using (5) and the initial gains obtained by using (7) at the instant of the disturbance for all cases. Each cell in Tables IV and V means the DFIG location. In all cases, if the rotor speed, ω_r, reaches $\omega_{\min}$, the inertial control schemes are disabled by disconnecting the additional inertial control loops. Table VI shows the outputs and reserve powers of SGs and a WPP prior to a disturbance.

TABLE IV

WIND SPEEDS FOR ALL CASES

Case 1 (m/s)				Case 2 (m/s)				Case 3 (m/s)			
Col.1	Col.2	Col.3	Col.4	Col.1	Col.2	Col.3	Col.4	Col.1	Col.2	Col.3	Col.4
10.00	9.06	8.97	8.95	8.00	7.25	7.18	7.16	13.00	11.78	11.67	11.63
10.00	9.06	8.97	8.95	8.00	7.25	7.18	7.16	13.00	11.78	11.67	11.63
10.00	9.06	8.97	8.97	8.00	7.25	7.18	7.18	13.00	11.78	11.67	11.67
10.00	9.06	9.06	9.06	8.00	7.25	7.25	7.25	13.00	11.78	11.78	11.78
10.00	10.00	10.00	10.00	8.00	8.00	8.00	8.00	13.00	13.00	13.00	13.00

Case 4 (m/s)				Case 5 (m/s)				Case 6 (m/s)				
Col.1	Col.2	Col.3	Col.4	Col.1	Col.2	Col.3	Col.4	Col.1	Col.2	Col.3	Col.4	Col.5
10.00	8.71	8.56	8.51	10.00	8.71	8.56	8.51	10.00	8.71	8.56	8.51	8.49
10.00	8.71	8.56	8.51	10.00	8.71	8.56	8.51	10.00	8.71	8.56	8.51	8.49
10.00	8.71	8.56	8.51	10.00	8.71	8.56	8.51	10.00	8.71	8.56	8.51	8.49
10.00	8.71	8.56	8.51	10.00	8.71	8.56	8.51	10.00	8.71	8.56	8.51	8.49
10.00	8.71	8.56	8.51	10.00	8.71	8.56	8.51	10.00	8.71	8.56	8.51	8.49
								10.00	8.71	8.56	8.51	8.49

TABLE V

INITIAL GAINS FOR ALL CASES

Case 1				Case 2				Case 3			
Col.1	Col.2	Col.3	Col.4	Col.1	Col.2	Col.3	Col.4	Col.1	Col.2	Col.3	Col.4
159	113	110	109	65	36	34	33	215	215	215	215
159	113	110	109	65	36	34	33	215	215	215	215
159	113	110	110	65	36	34	34	215	215	215	215
159	113	113	113	65	36	36	36	215	215	215	215
159	159	159	159	65	65	65	65	215	215	215	215

Case 4				Case 5				Case 6				
Col.1	Col.2	Col.3	Col.4	Col.1	Col.2	Col.3	Col.4	Col.1	Col.2	Col.3	Col.4	Col.5
159	96	90	89	159	96	90	89	159	97	91	89	89
159	96	90	89	159	96	90	89	159	97	91	89	89
159	96	90	89	159	96	90	89	159	97	91	89	89
159	96	90	89	159	96	90	89	159	97	91	89	89
159	96	90	89	159	96	90	89	159	97	91	89	89
								159	97	91	89	89

TABLE VI

OUTPUTS AND RESERVE POWERS OF GENERATORS FOR ALL CASES

	Output power (MW)/Reserve power (MW)					
	Case 1	Case 2	Case 3	Case 4	Case 5	Case 6
WPP	62/0	32/0	99/0	54/0	54/0	78/0
SG_1	77/73	84/66	67/83	77/73	77/73	77/73
SG_2	77/73	80/70	68/82	78/72	78/72	78/72
SG_3	94/106	106/94	91/109	99/101	99/101	98/102
SG_4	99/101	108/92	93/107	103/97	103/97	103/97
SG_5	70/30	70/30	70/30	70/30	70/30	70/30
SG_6	53/47	55/45	47/53	53/47	53/47	-

A. *Effects of Wind Speeds*

The inertial control capability of a WPP depends on the KE stored in the DFIGs. Thus, this subsection describes the effects of high (13 m/s), medium (10 m/s), and low (8 m/s) wind speeds with 45° wind direction on the performance of inertial control.

Case 1: Wind Speed of 10 m/s and Wind Direction of 45°

Fig. 9 illustrates the results for Case 1. In this case, the wind speed of $DFIG_1$ is 10 m/s, whereas the wind speeds of $DFIG_2$, $DFIG_3$, and $DFIG_4$ are 9.06 m/s, 8.97 m/s, and 8.95 m/s, respectively, as shown in Table IV. This means that the DFIGs in the first column and fifth row have the largest KE, whereas other DFIGs have the smaller KE.

As shown in Fig. 9(a), the FN of the small FGS is 0.13 Hz higher than that for "no inertial control" but 0.11 Hz lower than that in the large FGS, and 0.15 Hz lower than that in the AGS. The large and small gains are selected to ensure stable operation for all DFIGs while maximizing the inertial control performance in medium and low wind conditions; thus,

over-deceleration does not occur in the large and small FGSs (see Figs. 9(d) and 9(f)). The AGS also prevents the ω_i of all DFIGs from reaching ω_{min} no matter how much KE they have. This is done by reducing the gains depending on the temporally decreasing KE, as shown in Fig. 9(g).

Note that in the proposed AGS the power output of all DFIGs is confined by the torque limit, as shown in Figs. 9(c) and 9(e). Conversely, in the small FGS, the DFIGs release smaller additional power than that in the large FGS and the AGS only during the early stage of an event even though the DFIGs have enough KE; thus, the small FGS provides a limited contribution to improving the FN.

ω_1 in the AGS converges to a smaller value than in the large FGS because in the AGS, more KE from $DFIG_1$ is released than in the large FGS. Conversely, ω_4 in the AGS converges to a larger value than in the large FGS because in the AGS less KE from $DFIG_4$ is released than in the large FGS. The output and ω_i of $DFIG_2$ and $DFIG_3$ are similar to those of $DFIG_4$, and thus they are not shown herewith.

As shown in Fig. 9(g), the adaptive gain has a large value at the initial stage of an event, depending on the spatially different level of KE, and the initial gains of the four DFIGs are larger than that of the large FGS; then they temporally decrease with the square of ω_i. This helps ω_i converge to a value within the stable operating region. In addition, the adaptive gain of $DFIG_1$ decreases slower than that of $DFIG_2$, $DFIG_3$, and $DFIG_4$, because the released KE of $DFIG_1$ is smaller than that of the other DFIGs. This is because the output of $DFIG_1$ is confined by the torque limit. Therefore, the proposed AGS can improve the FN by setting spatially different gains to the DFIGs, and it can prevent over-deceleration by temporally reducing the gains with the KE.

Case 2: Wind Speed of 8 m/s and Wind Direction of 45°

Fig. 10 shows the results for Case 2, which is identical to Case 1 except for the lower wind speed. Thus, the WPP has less KE than that in Case 1. In this case, system frequency in the large FGS reduces at a slower rate than in the small FGS and the AGS, because the large FGS releases more power during the initial stage of an event (see Fig. 10(b)). In this case, the initial gains of the downstream DFIGs in the AGS are smaller than the gain of the large FGS. In the large FGS, the ω_i of all DFIGs reaches ω_{min}, even in $DFIG_1$, which has the largest KE. The additional loops in $DFIG_1$ and $DFIG_4$ are disabled at 48.1 s and 44.2 s, respectively, and thus their outputs significantly decrease. Thus, the WPP output abruptly decreases at 44.2 s. This will cause a subsequent frequency dip and the second FN is 59.57 Hz, which is 0.06 Hz smaller than the first FN. Afterward, the WPP output abruptly decreases at 48.1 s once again and the third frequency dip occurs and the third FN is 59.57 Hz. The small FGS ensures stable operation of all DFIGs, as in Case 1, but it still gives a limited contribution; thus, the FN is 0.05 Hz lower than it is in the AGS.

In this case, ω_1 in the AGS converges to a smaller value than in the small FGS, whereas ω_4 in the AGS converges to a larger value than in the small FGS.

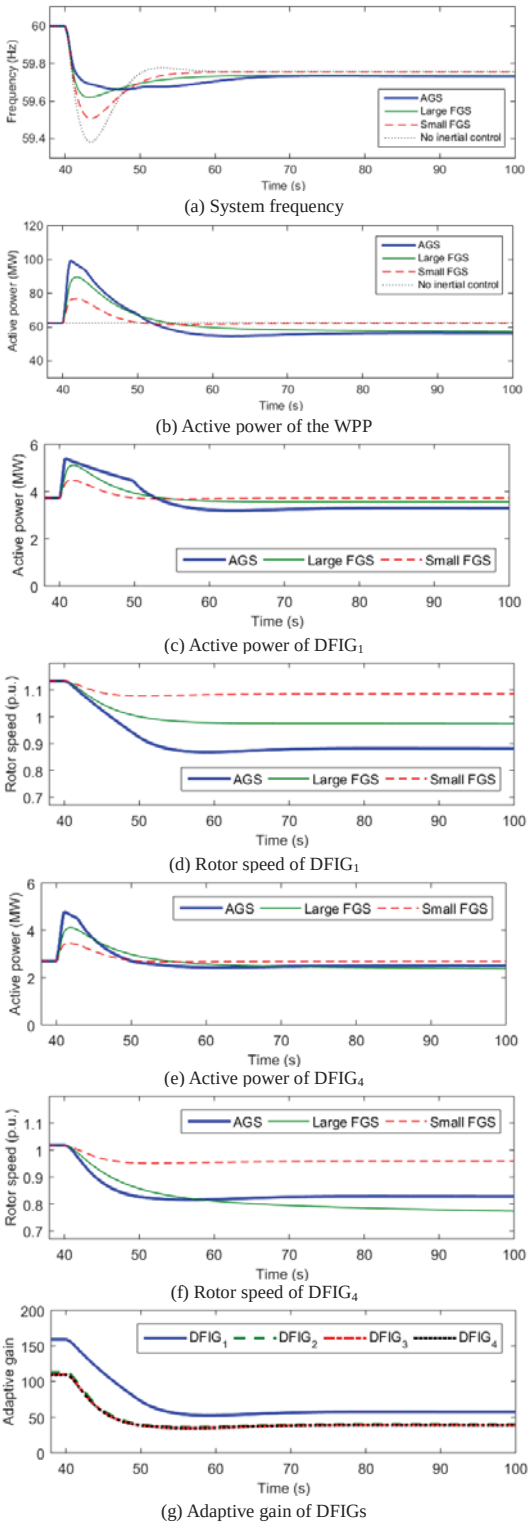

(a) System frequency
(b) Active power of the WPP
(c) Active power of $DFIG_1$
(d) Rotor speed of $DFIG_1$
(e) Active power of $DFIG_4$
(f) Rotor speed of $DFIG_4$
(g) Adaptive gain of DFIGs

Fig. 9. Results for Case 1

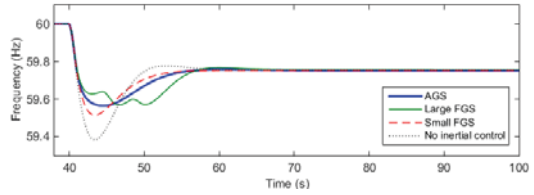

(a) System frequency

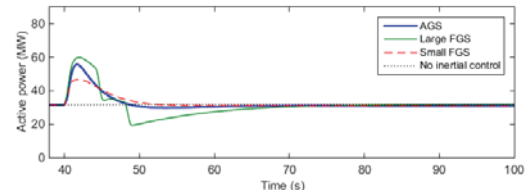

(b) Active power of the WPP

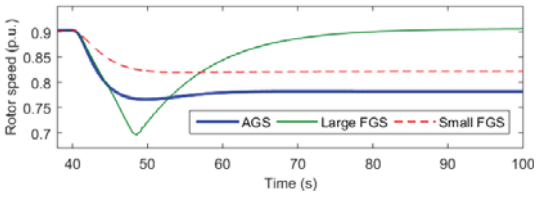

(c) Rotor speed of $DFIG_1$

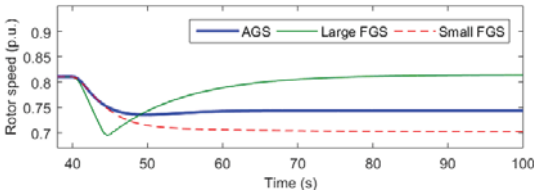

(d) Rotor speed of $DFIG_4$

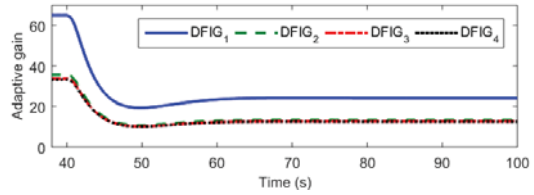

(e) Adaptive gain of DFIGs

Fig. 10. Results for Case 2

Even though the initial gain of $DFIG_1$ in the AGS is 1.4 times bigger than that of the large FGS, the AGS prevents ω_1 from reaching ω_{min} by reducing the adaptive gain. Thus, no second frequency dip appears. In this case, the AGS provides less KE than in Case 1, and thus the FN decreases to 59.57 Hz, which is 0.09 Hz smaller than it is in Case 1. This is because the KE in Case 2 is smaller. In addition, the adaptive gain of $DFIG_1$ decreases faster than that in Case 1.

Case 3: Wind Speed of 13 m/s and Wind Direction of 45°

Fig. 11 shows the results for Case 3, in which the wind speeds of DFIGs exceed the rated wind speed and all DFIGs operate in the full load region (see Table IV). In this case, the KE prior to a disturbance is the largest. As shown in Table V, the initial gains of all DFIGs are set to be maximum value of 215 because prior to a disturbance, they are operating at the same rotor speed of 1.25 p.u. (see Figs. 11(c) and 11(e)).

The FNs of the large FGS and AGS are 0.18 Hz higher than that of "no inertial control" and 0.03 Hz higher than that of the small FGS. The contribution of the large FGS and AGS to improving the FN is the same because the WPP outputs during

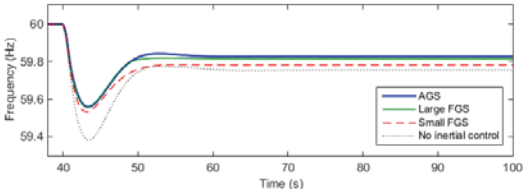

(a) System frequency

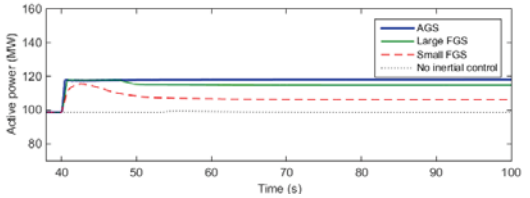

(b) Active power of the WPP

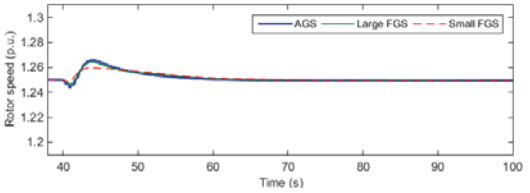

(c) Rotor speed of $DFIG_1$

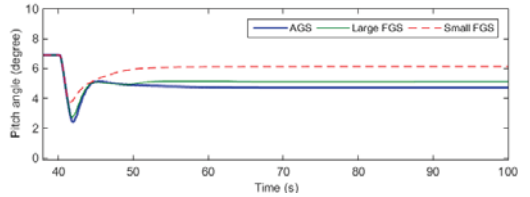

(d) Pitch angle of $DFIG_1$

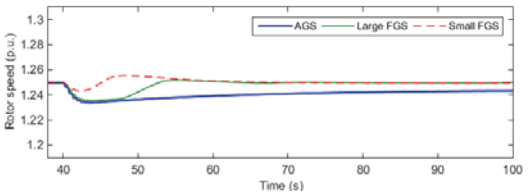

(e) Rotor speed of $DFIG_4$

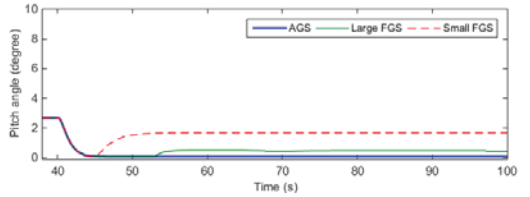

(f) Pitch angle of $DFIG_4$

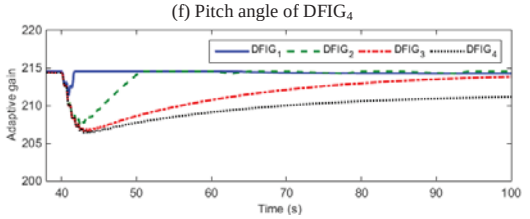

(g) Adaptive gain of DFIGs

Fig. 11. Results for Case 3

the initial stage of the disturbance are the same. Unlike the previous cases, in the proposed scheme the WPP keeps providing the active power of 1.2 p.u., which is the power limit of the DFIG, for a long duration because the curtailed power is released by reducing the pitch angle (see Figs. 11(d) and 11(f)). Thus, in this case, the frequency is stabilized to a higher value than those in Case 1 and Case 2.

After the disturbance, ω_1 increases after the short decrease and then exceeds 1.25 p.u. because the pitch angle reduction increases the mechanical input power of the DFIG. After a while, ω_1 returns to 1.25 p.u. In contrast, ω_4 in the proposed scheme decreases and is kept at a value smaller than 1.25 p.u.; then ω_4 keeps increasing while the pitch angle is kept at zero.

As shown in Fig. 11(g), the adaptive gain of $DFIG_1$ is returned to the maximum value after a short period. In contrast, the gains of $DFIG_2$, $DFIG_3$, and $DFIG_4$ return to the maximum value when ω_i returns to ω_{max}.

The results of the above three cases clearly indicate that the AGS can improve the FN by setting the spatially dependent gains to DFIGs, and it can prevent over-deceleration of all DFIGs by temporally reducing the gains with the declining KE under the high, medium, and low wind conditions.

B. Effects of Varying Wind Speeds

The performance of inertial control is critically dependent on the stored KE, which can be decreased because of a decrease in the wind speed and as a result of inertial control. Thus, as an example of extreme cases, this subsection describes the test results for two cases in which the wind speed decreases from high to a lower wind speed and using different intervals at the instant of a disturbance.

Case 4: Decreasing Wind Speed from 10 m/s to 7 m/s for 10 s and Wind Direction of 0°

Fig. 12 shows the result for Case 4, in which the free wind speed to the WPP starts decreasing at 40 s from 10 m/s to 7 m/s for 10 s. However, as shown in Fig. 12(a), because of the travel time of the wake wind, only $DFIG_1$ experiences the wind speed reduction during the simulation time.

Because of the wind direction change to 0°, the WPP has less KE than in Case 1 prior to an event. In the large FGS, the decreasing wind speed causes $DFIG_1$ to decelerate faster than in Case 1 (see Fig. 12(e)); unlike Case 1, ω_1 reaches ω_{min} at 54.3 s because of the wind speed reduction. At that instant, a second frequency dip starts because inertial control of $DFIG_1$ is disabled. Note that in this case, ω_4 reaches ω_{min} at 57.1 s unlike Case 1. The reason for this is as follows. The output of $DFIG_1$ decreases faster than in Case 1 because of the wind speed reduction; this can be seen by comparing Figs. 9(c) and 12(d). This causes further decrease of system frequency than that in Case 1. That is why $DFIG_4$ releases more power than in Case 1 and thus ω_4 decreases more rapidly (see Figs. 12(f) and 12(g)). The third FN is 59.51 Hz, which is 0.11 Hz smaller than the first FN. In the small FGS, ω_1 also reaches ω_{min} at 70.2 s because of the wind speed reduction; thus, the small FGS does not ensure stable operation in this case.

Because of faster ω_1 reduction than in Case 1, the AGS reduces the gain more quickly (see Fig. 12(h)); ω_1 eventually converges to 0.73 p.u., which is in the stable region. The FN of the AGS is 59.60 Hz, which is 0.09 Hz higher than that of the large and small FGSs. Note that in this case, $AG_1(\omega_1)$ becomes smaller than those of the other DFIGs after 49.7 s, because ω_1 decreases faster than in Case 1 because of the wind speed reduction and inertial control.

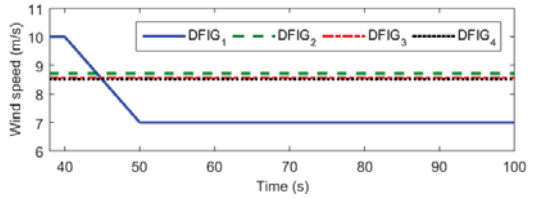

(a) Wind speed of DFIGs

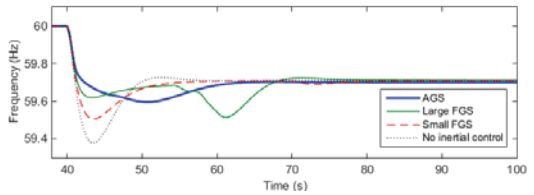

(b) System frequency

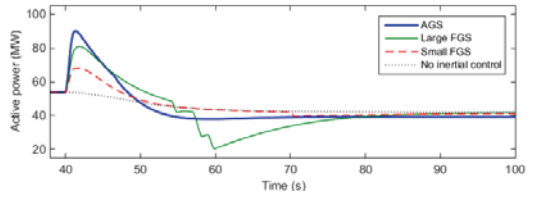

(c) Active power of the WPP

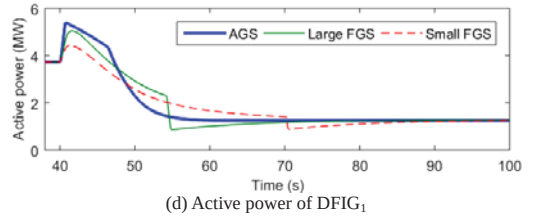

(d) Active power of $DFIG_1$

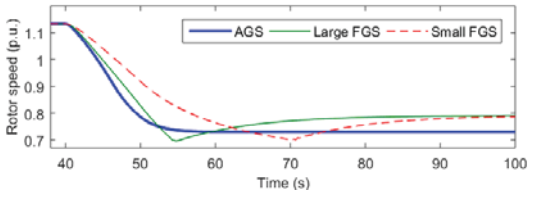

(e) Rotor speed of $DFIG_1$

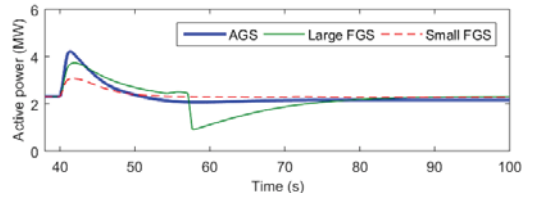

(f) Active power of $DFIG_4$

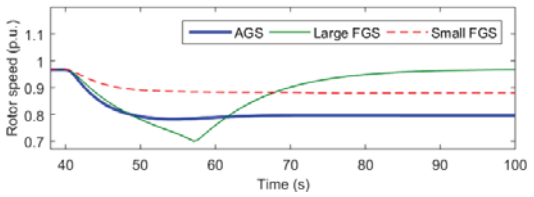

(g) Rotor speed of $DFIG_4$

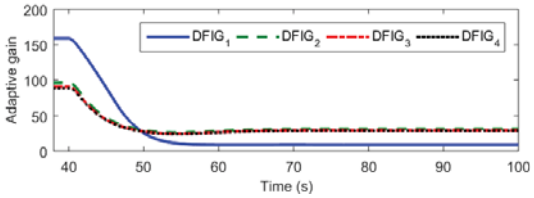

(h) Adaptive gain of DFIGs

Fig. 12. Results for Case 4

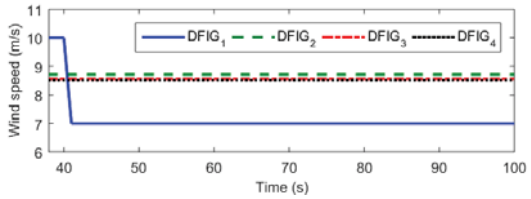

(a) Wind speed of DFIGs

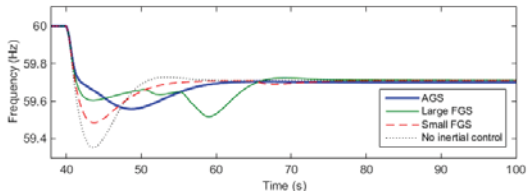

(b) System frequency

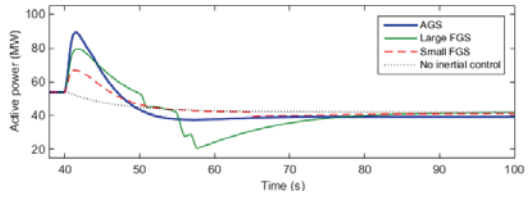

(c) Active power of the WPP

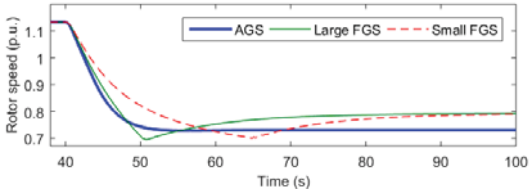

(d) Rotor speed of $DFIG_1$

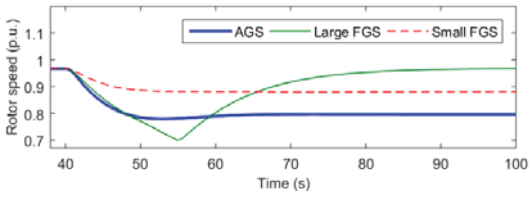

(e) Rotor speed of $DFIG_4$

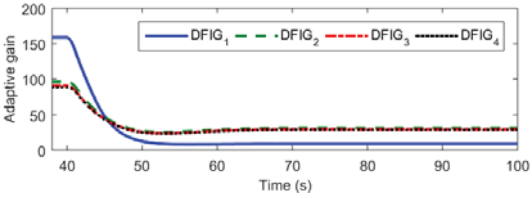

(f) Adaptive gain of DFIGs

Fig. 13. Results for Case 5

Case 5: Decreasing Wind Speed from 10 m/s to 7 m/s for 1 s and Wind Direction of 0°

Fig. 13 shows the results for Case 5. In this case, the wind speed decreases at 40 s from 10 m/s to 7 m/s for 1 s. The more rapid wind speed reduction than in Case 4 reduces ω_1 faster than in Case 4. Thus, the AGS reduces the WPP output faster than in Case 4 to ensure stable operation of all DFIGs, and system frequency is lower than in Case 4. As in the previous cases, the AGS ensures stable operation of all DFIGs. Conversely, in the large FGS, ω_1 and ω_4 reach ω_{min} at 50.3 s, and 54.9, respectively, which are 4.0 s and 2.2 s earlier than in Case 4; thus, subsequent frequency dips appear earlier. In the small FGS, ω_1 reaches ω_{min} at 64.9 s, which is 5.3 s earlier than in Case 4 because of the rapid wind speed decrease, and thus it is unable to ensure stable operation of all DFIGs. However, the AGS successfully prevents over-deceleration even in this case by rapidly reducing the gain, as shown in Fig. 13(f); thereby ω_1 converges to 0.73 p.u., which is also within the stable operating region.

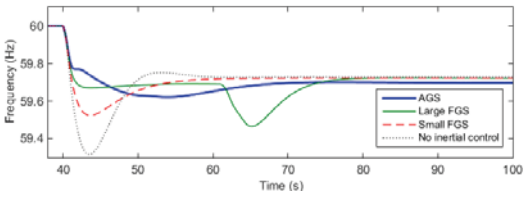

(a) System frequency

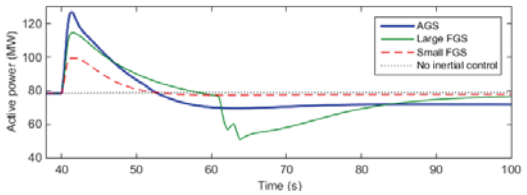

(b) Active power of the WPP

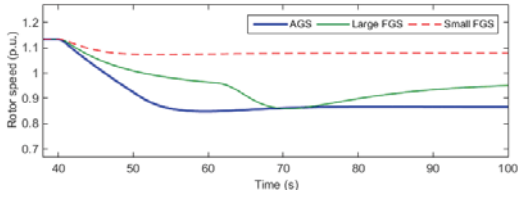

(c) Rotor speed of $DFIG_1$

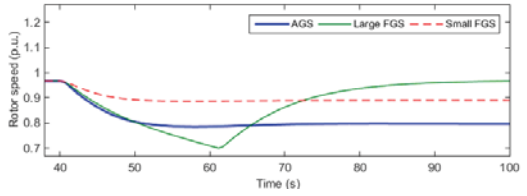

(d) Rotor speed of $DFIG_4$

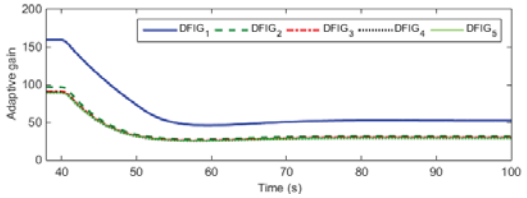

(e) Adaptive gain of DFIGs

Fig. 14. Results for Case 6

The results of Case 4 and Case 5 demonstrate that the AGS ensures stable operation of all DFIGs within the WPP while improving the FN even when the wind speed significantly decreases at the instant of a disturbance.

C. *Effects of Different System and WPP Configuration*

This subsection describes the investigation results of the proposed scheme for different system inertia and wind power penetration level. To do this, the number of DFIGs is increased, whereas the number of SGs is reduced.

Case 6: Wind Speed of 10 m/s, Wind Direction of 0 °, and Wind Power Penetration Level of 30%

In this case, the installed capacity of a WPP increases from

100 MW to 150 MW; to do this, one row and column of the WPP in the model system were added. In addition, the active load consumption decreases from 529 MW to 499 MW. Further, SG_6 is not operating and only five SGs are operating.

Fig. 14 shows the results for Case 6. The FN of "no inertial control" is 59.32 Hz, which is lower than those in the previous cases because of the smallest system inertia. In the large FGS, the first FN is 59.67 Hz. However, a second frequency dip occurs at 61.1 s caused by the disablement of the inertial control loop of $DFIG_4$; the second FN is 59.47 Hz, which is smaller than that of the small FGS. The AGS has the highest FN, which is 59.62 Hz, and also ensures stable operation of all DFIGs as in the previous cases.

V. Conclusion

This paper proposes a stable inertial control scheme based on adaptive gains for a DFIG-based WPP. To improve the FN, at the instant of an event, high gains are initially set to be proportional to the spatially different levels of KE stored in the DFIGs prior to an event; then, to ensure stable operation of all DFIGs, the gains decrease with the temporally declining KE.

The results clearly indicate that the proposed scheme shows better performance than the FGSs in terms of improving the FN and preventing over-deceleration under various wind and system conditions. Further, even when the wind speed decreases at the instant of an event, the AGS ensures stable operation of all DFIGs in a WPP.

The advantage of the scheme is that it improves the FN by using spatially dependent gains during the initial stage of an event; it reduces the gains with the temporally declining KE and thereby ensures stable operation of all DFIGs even when the wind speed decreases.

VI. Acknowledgment

This work was supported by the Ministry of Science, ICT, and future Planning (MSIP), Korea through the Wind-energy Gate Adaptive Technologies (WeGAT) Center at the Chonbuk National University, and the U.S. Department of Energy under Contract No. DE-AC36-08-GO28308 with the National Renewable Energy Laboratory.

VII. Appendix

A. Generator Parameters

Rated voltage (kV) = 13.8, X_d (p.u.) = 1.028, X_d' (p.u.) = 0.34, X_d'' (p.u.) = 0.253, X_q (p.u.) = 0.654, X_q' (p.u.) = 0.653, X_q'' (p.u.) = 0.298, X_l (p.u.) = 0.15, R_a (p.u.) = 0.0025, T_{d0}' (s) = 7.5, T_{d0}'' (s) = 0.07, T_{q0}' (s) = 3.0, T_{q0}'' (s) = 0.09.

B. Transmission Line Parameters

R (Ω/km) = 0.3, L (mH/km) = 3, C (μF/km) = 0.008. Transmission line length (km): TL_1 = 200, TL_2 = 220, TL_3 = 220, TL_4 = 200, TL_5 = 150, TL_6 = 150.

VIII. References

[1] H. Bevrani, "Real power compensation and frequency control," in *Robust Power System Frequency Control*, Ed. New York: Springer Science+Business Media, LLC, 2009, pp. 15−37.

[2] B. Delfino, S. Massucco, A. Morini, P. Scalera, and F. Silvestro, "Implementation and comparison of different under frequency load-shedding schemes," presented at the IEEE Summer Meeting 2001, Vancouver, BC, Canada, Jul. 15−19, 2001.

[3] Hydro Québec., "Transmission provider technical requirements for the connection of power plants to the Hydro Québec transmission system," Hydro Québec., Montréal, Québec, Feb. 2009.

[4] J. Ekanayake and N. Jenkins, "Comparison of the response of doubly fed and fixed-speed induction generator wind turbines to changes in network frequency," *IEEE Trans. Energy Convers*., vol. 19, no. 4, pp. 800−802, Dec. 2004.

[5] G. Lalor, A. Mullane, and M. O'Malley, "Frequency control and wind turbine technologies," *IEEE Trans. Power Syst*., vol. 20, no. 4, pp. 1905−1913, Nov. 2005.

[6] M. Kayikçi and J. V. Milanovic, "Dynamic contribution of DFIG-based wind plants to system frequency disturbances," *IEEE Trans. Power Syst.*, vol. 24, no. 2, pp. 859−867, May 2009.

[7] J. Morren, J. Pierik, and S. W. H. de Haan, "Inertial response of variable speed wind turbines," *Elect. Power Syst. Res.*, vol. 76, no. 11, pp. 980−987, Jul. 2006.

[8] J. Morren, S. Haan, W. L. Kling, and J. A. Ferreira, "Wind turbines emulating inertia and supporting primary frequency control," *IEEE Trans. Power Syst.*, vol. 21, no. 1, pp. 433−434, Feb. 2006.

[9] G. Ramtharan, J. B. Ekanayake, and N. Jenkins, "Frequency support from doubly fed induction generator wind turbines," *IET Renew. Power Gener.*, vol. 1, no. 1, pp. 3−9, Mar. 2007.

[10] I. D. Margaris, S. A. Papathanassiou, N. D. Hatziargyriou, A. D. Hansen, and P. Sørensen, "Frequency control in autonomous power systems with high wind power penetration," *IEEE Trans. Sustain. Energy*, vol. 3, no. 2, pp. 189−199, Apr. 2012.

[11] J. F. Conroy and R. Watson, "Frequency response capability of full converter wind turbine generators in comparison to conventional generation," *IEEE Trans. Power Syst.*, vol. 23, no. 2, pp. 649−656, May 2008.

[12] J. V. D. Vyver, J. D. M. D. Kooning, B. Meersman, L. Vandevelde, and T. L. Vandoorn, "Droop control as an alternative inertial response strategy for the synthetic inertia on wind turbines," *IEEE Trans. Power Syst.*, vol. PP, no. 99, pp. 1−10, May 2015.

[13] V. Ajjarapu, J. D. McCalley, D. Rover, Z. Wang, and Z. Wu, "Novel sensorless generator control and grid fault ride-through strategies for variable-speed wind turbines and implementation on a new real-time simulation platform," Ph.D. dissertation, Dept. Elect. Eng., Iowa State Univ., Ames, Iowa, 2010.

[14] A. Petersson, "Analysis, modeling and control of doubly-fed induction generators for wind turbines," Ph.D. dissertation, Dept. of Energy Environ., Chalmers Univ. Technol., Göteborg, Sweden, 2005.

[15] J. M. Mauricio, A. Marano, A. Gómez-Expósito, and J. L. M. Ramos, "Frequency regulation contribution through variable-speed wind energy conversion systems," *IEEE Trans. Power Syst.*, vol. 24, no. 1, pp. 173−180, Feb. 2009.

[16] M. M. Hand, "Variable-speed wind turbine controller systematic design methodology: a comparison of non-linear and linear model-based designs," National Renewable Energy Laboratory, Golden, CO, NREL/TP-500-25540, Jul. 1999.

[17] I. Katic, J. Højstrup, and N. O. Jensen, "A simple model for cluster efficiency," in *Proc. 1986 European Wind Energy Association Conference and Exhibition*, Italy, Oct. 7−9, 1986.

[18] F. Koch, M. Gresch, F. Shewarega, I. Erlich, and U. Bachmann "Consideration of wind farm wake effect in power system dynamic simulation," in *Proc. 2005 Power Tech*, Russia, Jun. 27−30, 2005.

[19] Y. Wang, G. Delille, H. Bayem, X. Guillaud, and B. Francois, "High wind power penetration in isolated power systems—assessment of wind inertial and primary frequency responses," *IEEE Trans. Power Syst.*, vol. 28, no. 3, pp. 2412−2420, Feb. 2013.

[20] J. Sutter and C. Muriithi, "Analysis of power system transient stability due to increased integration of geothermal power," presented at the 39th Workshop on Geothermal Reservoir Engineering, Stanford, CA, Feb. 24−26, 2014.

[21] R. T. Byerly, O. Aanstad, D. H. Berry, R. D. Dunlop, D. N. Ewart, B. M. Fox, L. H. Johnson, and D. W. Tschappat, "Dynamic models for steam

and hydro turbines in power system studies," *IEEE Trans. Power App. Syst.*, vol. PAS-92, no. 6, pp. 1904−1915, Nov. 1973.
[22] P.-K. Keung, P. Li, H. Banakar, and B. T. Ooi, "Kinetic energy of wind-turbine generators for system frequency support," *IEEE Trans. Power Syst.*, vol. 24, no. 1, pp. 279−287, Feb. 2009.
[23] P. Kundur, "Power system loads," in *Power System Stability and Control*, Ed. New York: McGraw-Hill, 1994, pp. 271−313.

BIOGRAPHIES

Jinsik Lee (S'12) received the B.Sc. and M.Sc. degrees from Chonbuk National University, Korea, in 2011 and 2013. He is currently pursuing a Ph.D. degree at Chonbuk National University and is also an assistant researcher at the Wind energy Grid-Adaptive Technology (WeGAT) Research Center supported by the Ministry of Education, Science, and Technology, Korea. His research interests include plant-level control systems for wind power plants.

Gilsoo Jang (SM'06) received the B.S. and M.S. degrees in electrical engineering from Korea University, Seoul, Korea, in 1991 and 1994, respectively, and the Ph.D. degree in electrical and computer engineering from Iowa State University, Ames, IA, USA, in 1997. He is currently a professor with the School of Electrical Engineering, Korea University. He is an editor of the IEEE *Transactions on Smart Grid*. His current research interests include power quality and power system control.

Eduard Muljadi (F'10) received his Ph.D. in electrical engineering from the University of Wisconsin at Madison. In June 1992, he joined the National Renewable Energy Laboratory in Golden, Colorado. His current research interests are in the fields of electric machines, power electronics, and power systems in general, with an emphasis on renewable energy applications. He is an editor of the IEEE *Transactions on Energy Conversion*. He is involved in the activities of the IEEE Industry Application Society, Power Electronics Society, and Power and Energy Society.

Frede Blaabjerg (F'03) received the Ph.D. degree from Aalborg University, Aalborg, Denmark, in 1992. He was with ABB-Scandia, Randers, Denmark, from 1987 to 1988. He is a full professor of power electronics and drives. His current research interests include power electronics and its applications such as in wind turbines, PV systems, reliability, harmonics, and adjustable speed drives. He was an editor-in-chief of the IEEE *Transactions on Power Electronic* from 2006 to 2012.

Zhe Chen (SM'98) received the B.Eng. and M.Sc. degrees from the Northeast China Institute of Electric Power Engineering, Jilin City, China, and the Ph.D. degree from the University of Durham, Durham, U.K. He is currently a full professor with the Department of Energy Technology, Aalborg University, Denmark. His main current research interests are wind energy and modern power systems. Chen is an editor of the IEEE *Transaction on Power Systems* and an associate editor of the IEEE *Transactions on Power Electronics*.

Yong Cheol Kang (SM'13) received his B.Sc., M.Sc., and Ph.D. degrees in electrical engineering from Seoul National University, Korea, in 1991, 1993, and 1997, respectively. He has been with Chonbuk National University, Korea, since 1999. He is currently a professor at Chonbuk National University and the director of the WeGAT Research Center. He is currently a visiting scholar at the National Renewable Energy Laboratory in Golden, Colorado, and a member of the International Electrotechnical Commission 61400-27 working group. His research interests include the development of control and protection techniques for wind power plants.